



NAȚIONAL POLITECHNIC UNIVERSITY OF SCIENCE
AND TECHNOLOGY BUCHAREST
DOCTORAL SCHOOL OF ELECTRICAL ENGINEERING

DOCTORAL THESIS

Summary of the doctoral thesis

CRYOELECTROTECHNICAL METHODS FOR HIGH MAGNETIC FIELDS

Scientific coordinator

Prof. Dr. Ing. Alexandru – Mihail Morega

Author

Ing. Dumitru George

Content

STRUCTURE OF THE DOCTORAL THESIS CHAPTERS	5
INTRODUCTION	6
1. SUPERCONDUCTIVITY	7
1.1. INTRODUCTION	7
1.2. SUPERCONDUCTING STATE.....	7
1.3. SUPERCONDUCTING MATERIALS CLASSIFICATION	8
1.3.1. TYPE I SUPERCONDUCTING MATERIALS	8
1.3.2. TYPE II SUPERCONDUCTING MATERIALS	8
1.4. CLASSIFICATION OF SUPERCONDUCTING MATERIALS ACCORDING TO THE TEMPERATURE RANGE	8
1.4.1. LOW TEMPERATURE SUPERCONDUCTING MATERIALS (LTS)	9
1.4.2. HIGH TEMPERATURE SUPERCONDUCTING MATERIALS (HTS).....	9
1.5. THE MAIN APPLICATIONS OF SUPERCONDUCTING MATERIALS	9
1.5.1. ELECTRICAL TRANSPORT LINES	10
1.5.2. ELECTRICAL MACHINES.....	10
1.5.3. MEDICAL EQUIPMENTS	10
1.6. CONCLUSIONS.....	10
2. HIGH AND UNIFORM MAGNETIC FIELD GENERATOR.....	11
2.1. ITRODUCION	11
2.2. MAGNETIC FIELD ANALYSIS	11
2.2.1. SINGLE TURN COIL.....	11
2.2.2. MULTI TURN COIL	11
2.2.3. PANCAKE COIL.....	12
2.2.4. HELMHOLTZ COIL.....	12
2.3. EVALUATION OF HTS MATERIALS PARAMETERS.....	12
2.4. NUMERICAL EVALUATION OF THE MAGNETIC FIELD GENERATED BY THE HELMHOLTZ ASSEMBLY	13
2.4.1. MAGNETIC FIELD EVALUATION.....	13
2.4.2. MAGNETIC FIELD EVALUATION TROUGH NUMERICAL MODELING	14
2.5. CONCLUSIONS.....	15
3. THERMAL ANALYSIS PARAMETERS OF THE COOLING SYSTEM FOR THE SUPERCONDUCTING ELECTROMAGNET	16
3.1. INTRODUCTION	16
3.2. TRANSFER PHENOMENA AT LOW TEMPERATURES	16
3.2.1. THERMAL CONDUCTION	16
3.2.2. THERMAL RADIATION	16
3.2.3. THERMAL CONVECTION	17
3.3. COOLING METHODS	17
3.3.1. COOLING WITH CRYOGENIC AGENTS	17
3.3.2. HEAT PUMPS COOLING	17
3.4. SIZING THE COOLING SYSTEM FOR THE HTS SUPERCONDUCTING ELECTROMAGNET.....	18
3.4.1. THERMAL PARAMETERS OF THE CRYOSTAT-ELECTROMAGNET ASSEMBLY.....	18
3.4.2. RADIATIVE HEAT FLUX EVALUATION	19
3.4.3. CONDUCTIVE HEAT FLUX EVALUATION	19
3.5. CONCLUSIONS.....	21
4. REALIZATION AND TESTING OF THE SUPERCONDUCTING ELECTROMAGNET.....	22
4.1. INTRODUCTION	22
4.2. MECHANICAL STRUCTURE OF THE ELECTROMAGNET.....	22
4.3. SUPERCONDUCTING COILS EXECUTION	22
4.3.1. JUNCTION OF SUPERCONDUCTING HTS TYPE	23

4.3.2.	CURRENT SUPPLY CONDUCTORS.....	24
4.3.3.	ELECTROMAGNET REALIZATION.....	24
4.4.	CRYOGENIC COOLING SYSTEM.....	25
4.4.1.	CRYOSTAT	25
4.4.2.	THERMAL SHIELD	25
4.5.	EXPERIMENTAL TESTS	25
4.5.1.	TESTING THE HTS TAPES	26
4.5.2.	HTS ELECTROMAGNET TESTING SYSTEM	27
4.5.3.	EXPERIMENTAL RESULTS.....	27
4.6.	CONCLUSIONS.....	29
5.	CONCLUSIONS.....	30
C.1.	GENERAL CONCLUSIONS	30
C.2.	ORIGINAL CONTRIBUTIONS	31
C.3.	DEVELOPMENT PERSPECTIVES	31
6.	BIBLIODRAPHY	32

Keywords: superconductivity, high magnetic field, high uniformity, heat transfer, numerical modeling, HTS conductors, superconducting junctions, cryogenic temperatures, cryogenic agents, heat pumps, design, cryostat, thermal shield.

STRUCTURE OF THE DOCTORAL THESIS CHAPTERS

The doctoral thesis entitled "Cryoelectrotechnical methods for high magnetic fields", is structured in 4 chapters, conclusions and bibliography, and will present the methods to design and develop a uniform high magnetic field generator using high temperature superconducting materials. Considering the fact that the field values required to achieve the demands of the application in which this magnetic field generator needs to be used exceed the conventional capabilities of conventional conductors, magnetic fields of up to 2,5 T can be obtained, the use of superconducting materials is required, to overcome this limitation. In order to achieve this goal, on the one hand, a rigorous evaluation of the phenomena associated with the superconducting state, as well as the characteristics of commercially existing materials is necessary, so that the selection of the materials to be used corresponds to the performances for which this generator will be designed.

Thus, in Chapter 1, called "SUPERCONDUCTIBILITY (CHARACTERISTICS AND PERFORMANCES)", the main performances and characteristics of superconducting materials used in industry, their evolution over time, and also how they become indispensable in the last decades in the devices development, from various fields will be presented.

In Chapter 2, entitled "INTENSE AND UNIFORM MAGNETIC FIELD GENERATORS", the technical solutions for magnetic field generators developed with this type of superconducting materials are presented, as well as the development of a conceptual model for such an electromagnet.

Chapter 3, entitled "ANALYSIS OF THE THERMAL PARAMETERS OF THE COOLING SYSTEM FOR A SUPERCONDUCTING ELECTROMAGNET" deals with the heat transfer problems associated with equipment using superconducting materials, in order to ensure their operating thermal parameters.

In Chapter 4, entitled "REALIZATION AND TESTING OF A SUPERCONDUCTING ELECTROMAGNET", are presented the execution stages, testing methods, and the experimental results obtained from the tests carried out of the superconducting electromagnet.

INTRODUCTION

The applications of superconducting materials have expanded in recent decades in many fields such as electrical engineering, through the creation of power lines, whose performance are clearly superior to conventional transmission lines [1], high power transformers [2, 3], current limiters that protects the power lines [4], magnetic field energy storage systems [5]. In the medical industry, these materials have led on the one hand to the development of facilities for magnetic resonance investigations [6], as well as the development of new methods for investigations such as magnetoencephalography [7]. In the transport industry, superconducting materials have been imposed due to the possibility of developing high-speed trains that use magnetic levitation, exceeding the maximum speed that can be reached by conventional methods [8].

Another field in whose development superconducting materials play an significant role is that of applied physics, the use of superconducting materials making possible the development of large particle accelerators that can develop energies of up to 14 TeV [9]. Due to the superior performance of the new high temperature superconducting materials generically called High Temperature Superconductor (HTS) developed in the last decades, the possibility of obtaining high magnetic fields, which can reach tens of T [10] opened new possibilities in this field.

The development of high and uniform magnetic field generators using high-temperature superconducting materials requires, on the one hand, a deep knowledge of these types of materials, but also of the restrictions imposed by them, restrictions corelated low temperatures at which they are used.

Design of such high and uniform magnetic field generator made with HTS superconducting materials for applications in spectroscopy, its realization method, as well as the experimental results obtained, presented in this work, aim to overcome the limitations imposed by the use of conventional conducting materials for this type of application.

1. SUPERCONDUCTIVITY

1.1. INTRODUCTION

The use of superconducting materials in practical applications has demonstrated through their performance that they become indispensable for technological progress. The use of this type of materials implies a deep knowledge of their properties and implicitly of the phenomena that govern the superconductivity state. In this chapter a brief presentation of the superconducting state of materials, their associated properties and the main parameters that must be taken into account for practical applications is presented. In the second part of this chapter, the main applications of these types of superconducting materials that have been imposed in the last decades in many fields of activity are briefly presented.

1.2. Superconducting state

The superconductivity state was discovered by Heike Kamerlingh Onnes in 1911 [11]. When the temperature of the studied material is kept below a value called the critical temperature (T_c), it shows zero electrical resistance, rising the possible to electric current transport without Joule losses.

In 1933, Walther Meissner și Robert Ochsenfeld [13] have highlighted the fact that this material at a temperature below the critical temperature (T_c), when is placed in a constant and uniform magnetic field, a superconducting current spontaneously appears at the surface, shielding the material from the external magnetic field, the material behaving like a perfect diamagnet, (the Meissner–Ochsenfeld effect) [12, 14]. The equations describing the Meissner effect were proposed in 1935 by Fritz Wolfgang London and Heinz London brothers [11]. According to them, an external magnetic field B_0 , parallel to a superconducting material will not be completely attenuated at the material interface, it will be attenuated according to the relation [11]:

$$B(x) = B_0 e^{-\left(\frac{x}{\lambda_L}\right)}, \quad (1)$$

where $B(x)$ is the magnetic field inside the superconducting material. The London penetration depth of the magnetic field in the material λ_L , is [11, 15, 16]:

$$\lambda_L = \sqrt{\frac{m_e}{\mu_0 n e^2}}. \quad (2)$$

An external current applied to the superconducting material will only flow in the region determined by the penetration depth [11, 15]. The penetration depth of the magnetic field inside the superconducting material is dependent on the temperature, its variation being [15]:

$$\lambda_L(T) = \frac{\lambda_L(0)}{\left[1 - \left(\frac{T}{T_c}\right)^4\right]^{1/2}}, \quad (3)$$

where $\lambda_L(0)$ is the penetration depth at $T = 0$ K. In the superconducting state, the transport current is carried out by electrons grouped in pairs (Cooper pairs) [17]. The charge carriers volume density variation, from the material surface to its center is characterized by the coherence length ξ [11, 14].

1.3. Superconducting materials classification

Depending on the behavior in the magnetic field, superconducting materials are classified into two categories, type I superconducting materials and type II superconducting materials.

The difference between type I and type II materials is given by the penetration depth and coherence length ratio, $k = \lambda_L/\xi$, where k is Ghinzburg-Landau parameter [15], $k < 1/\sqrt{2}$ for type I materials, and $k > 1/\sqrt{2}$ for type II respectively [11].

Critical temperature (T_c) is another parameter by which the classification is made, differentiating three categories:

- LTS (Low Temperature Superconductor);
- MTS (Medium Temperature Superconductor);
- HTS (High Temperature Superconductor).

1.3.1. Type I superconducting materials

For a type I superconducting material at temperature T , where $T < T_c$, if an external current is applied, will flow only through the region corresponding to the penetration depth λ_L [11, 15]. For an external current applied to the material in the superconducting state, whose density J_{ext} exceeds the current density J_{sc} , the material will make the transition from the superconducting state to normal state, the maximum external current supported by this material is called the critical current (I_c). The maximum external magnetic field up to which the superconductivity state can be maintained is called critical field B_c and has the form [15]:

$$B_c(0) = \mu_0 \lambda(0) J_c(0), \quad (4)$$

where $B_c(0)$ and $J_c(0)$ are the critical magnetic field and critical current density for $T = 0$. The critical magnetic field as a function of temperature $B_c(T)$, is [15]:

$$B_c(T) = B_c(0) \left[1 - \left(\frac{T}{T_c} \right)^2 \right]. \quad (5)$$

1.3.2. Type II superconducting materials

Type II superconductors exhibit a lower critical field B_{c1} , and an upper critical field denoted B_{c2} . For $0 < B < B_{c1}$, the behavior of these materials is similar to that of type I. For $B_{c1} < B < B_{c2}$, the magnetic field partially penetrates the material, thus a mixed zone called the Shubnikov region appears [18]. The behavior of type II superconducting materials was described in 1957 by the A. Abrikosov [18]. If the superconducting material is between B_{c1} and B_{c2} , the external magnetic field will partially penetrate the superconducting material through regions called fluxons, around which supercurrents appears [14], these being characterized by the penetration depth λ_L and the coherence length ξ . Inside these fluxons, the superconducting state disappears, the material is normal conductor, but in the region between them, the material is superconducting.

1.4. Classification of superconducting materials according to the temperature range

At present, the common superconducting materials are divided according to the temperature range into three categories: LTS low temperature superconducting materials whose critical temperature T_c is in the range of 2 K to 19 K, medium-temperature

superconducting materials with the critical temperature in the range $19 \text{ K} < T_c < 77 \text{ K}$ and HTS high temperature superconducting materials, whose critical temperature T_c is in the range between 90 K and 135 K.

1.4.1. Low temperature superconducting materials (LTS)

For practical applications, NbTi-type alloys have been developed in the form of filaments embedded in copper support, this support providing both mechanical strength and high thermal conductivity. An example of this is the superconductor used to develop the coils for LHC particle accelerator, the conductors used having 0.48 mm and 0.82 mm diameter respectively, supporting an external magnetic field of up to 11 T [20]. In practice, to choose the superconducting material, we must take into account its critical parameters: critical temperature T_c , critical field B_c and critical current density J_c . Figure 3 shows the variation of the three critical parameters for some superconducting materials. The surface described by these parameters represents the critical surface of the superconducting material [14].

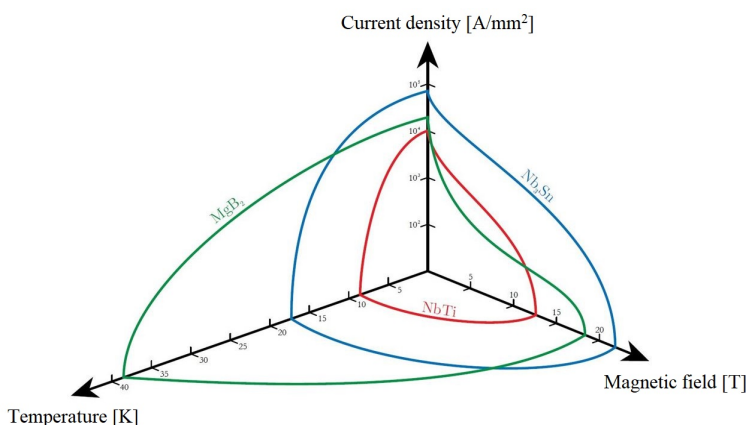


Fig. 3. Critical surface of superconducting materials [14].

1.4.2. High temperature superconducting materials (HTS)

In 1986 when Johannes Georg Bednorz and Karl Alexander Müller discovered the BaLaCuO matrix which, at a temperature of 35 K, becomes superconducting [21]. Later, superconducting materials with a critical temperature T_c of up to 107 K were developed, making possible the use of liquid nitrogen as a cryogenic agent. The most widespread HTS materials are BiSrCaCuO, discovered in 1988, with a critical temperature between 85 K and 110 K, and a critical field of maximum 200 T [14], and materials made with rare earths such as YBaCuO and GdBaCuO with a critical temperature of 92 K and a critical field of up to 140 T [14].

1.5. The main applications of superconducting materials

Despite the low cost of LTS-type materials ($\sim 5 \text{ \$/KA}\cdot\text{m}$) [22], the applications developed with this type of material have been limited. The discovery of HTS-type materials has broadened the applications spectrum of the field of electrical engineering, making possible the use of them in many fields. Due to the fact that the manufacturing the HTS superconducting materials is complex and expensive compared to that of LTS materials, their cost was high, initially exceeding $1000 \text{ \$/KA}\cdot\text{m}$ [23].

1.5.1. Electrical transport lines

An example of an transport line is the conductor produced by Cryogenic and Vacuum Engineering (CVE) [24], with a total length of 1000 m, a working voltage of 154 kV, and temperature range of 70 – 80 K [24]. For the use of HTS materials in applications where the current density exceeds the current density supported by a single strip, it is necessary to make a conductor consisting of multiple HTS strips, arranged in a construction called Roebel cable [25]. Robinson Research Institute engineers developed for the first time a full automated device that can produce such a conductor [26].

1.5.2. Electrical machines

The sustained efforts in the development of electric machines using HTS materials have materialized through the development, within the Laboratory of Applied Superconductivity of National Institute for Research and Development in Electrical Engineering ICPE-CA of a three-phase superconducting generator made with HTS superconducting materials, this having a nominal speed of 1000 rpm and a maximum power of 1000 rpm, and 4,5 kW power [28].

1.5.3. Medical equipments

Development of electromagnets with superconducting materials made possible the development of Nuclear Magnetic Resonance Imaging (NMR) scanning equipment, changing the way medical investigations are carried out. Also in the medical field, superconducting materials can be used to make magnetic sensors called SQUID (Superconducting Quantum Interference Device) capable of measuring magnetic field gradients with a resolution of the order of 10^{-12} T/m [27], this sensors been used in investigation called magnetoencephalography.

1.6. Conclusions

In this chapter, the superconducting state and the fundamental characteristics of superconducting materials (T_c , I_c and B_c) were presented, as well as the temperature dependence of the last two parameters, and the main aspects of the London and Abrikosov models on superconductivity were reviewed. Superconducting materials with practical applicability, both LTS and HTS type, were also presented, highlighting both the advantages and disadvantages of each category. High temperature superconducting materials have been shown to be superior to low temperature superconducting materials in terms of critical temperature, critical current and critical field. The main applications of the HTS superconducting materials presented in this chapter, some of which were also developed within the Laboratory of Applied Superconductivity in Electrical Engineering of ICPE-CA [28], through the performances achieved, demonstrates the necessity of using these types of materials in order to fulfill the objectives of this work.

2. HIGH AND UNIFORM MAGNETIC FIELD GENERATOR

2.1. ITRODUCION

The main objective of the present work is the design of an electromagnet made with high temperature superconducting materials (HTS), with applications in nuclear spectroscopy. For the design of such a superconducting electromagnet, it is necessary to take into account the restrictions imposed by the application in which it will be used. The main parameters imposed by the application are the maximum magnetic field generated, the geometric parameters of the field area and the spatial uniformity of the field. In the design process of superconducting electromagnets, certain constraints imposed both by the performance to be achieved, but also by the functional characteristics of the superconducting materials (critical parameters of the material) will be taken into account. The electric and magnetic parameters of the electromagnet can be calculated conventionally, using the electromagnetism equations, but the limitations imposed by the parameters of the superconducting material used will be applied.

2.2. Magnetic field analysis

2.2.1. Single turn coil

The magnetic field at any point P located at distance R' along z axis of a single turn coil of radius r , carried by current I is [16, 29]:

$$H_z = \frac{Ir^2}{2\sqrt{(r^2 + R'^2)^3}}. \quad (8)$$

2.2.2. Multi turn coil

To evaluate the magnetic field generated by a real coil, the dimensionless parameter λ must be entered, this represents the ratio between the actual section of the conductor used and the total section including the insulator, this being called the fill factor.

Considering a coil with a uniform current density, with the inner radius r_1 , the outer radius r_2 , the total height $2h$ and the number of turns N , we can determine the the magnetic field in the center of the coil generated by the stationary current I passing through the elementary area dA :

$$dB_z(0,0) = \frac{\mu_0 r^2 \lambda J dA}{2\sqrt{(r^2 + R'^2)^3}}, \quad (9)$$

were J [A/m²] is the current density and A [mm²] is the conductor's area. Product between fill factor λ and current density J is [16]:

$$\lambda J = \frac{NI}{2h(r_2 - r_1)} \quad (10)$$

Introducing the dimensionless parameters $\alpha = r_2/r_1$ și $\beta = h/r_1$, the magnetic field in center of the coil is [16]:

$$B_z(0,0) = \mu_0 \lambda J r_1 \beta \ln \left(\frac{\alpha + \sqrt{\alpha^2 + \beta^2}}{1 + \sqrt{1 + \beta^2}} \right). \quad (11)$$

Adding the field factor $F(\alpha, \beta)$, the equation (11) become [30]:

$$B_z(0,0) = \mu_0 \lambda J r_1 F(\alpha, \beta). \quad (12)$$

2.2.3. Pancake coil

Making superconducting materials with the shape of tape can be a limitation in the design of certain geometries depending on the application in which they will be used. A restrictive parameter of this type of material is the minimum bending radius (\sim cm). Due to the limitations imposed by the geometry of the superconducting materials, it is necessary to make the coils in the pancake shape, but for this configuration β becomes very small.

2.2.4. Helmholtz coil

In order to generate a magnetic field with high uniformity in a certain distance, along Oz axis, a coil system in the Helmholtz configuration is considered, consisting of two identical coils of radius r , placed coaxially at a distance h from each other, the first coil being aligned on the z axis at a distance $z = h/2$, and the second coil being at a distance $z = -h/2$. The magnetic field generated by the two coils at a point along the z axis is [16]:

$$H_z(0, z) = \frac{I r^2}{2} \left\{ \left[r^2 + \left(z + \frac{h}{2} \right)^2 \right]^{-3/2} + \left[r^2 + \left(z - \frac{h}{2} \right)^2 \right]^{-3/2} \right\}. \quad (13)$$

A condition imposed by the application for which the superconducting electromagnet is to be used, is the generation of a magnetic field with high uniformity in a certain region along the Oz -axis, access direction to the uniform magnetic field area being another condition imposed by which must be taken into account when choosing the configuration of the electromagnet. Thus, the electromagnet model that can satisfy both conditions is represented by Helmholtz configuration coils.

2.3. Evaluation of HTS materials parameters

In order to develop the superconducting electromagnet, an analysis of the superconducting materials available on the market is required. The most important companies producing these type of superconducting materials are [31]: Theva Dünnschichttechnik GmbH [32], FURUKAWA ELECTRIC GROUP (Superpower) [33], AMSC [34], FARADAY FACTORY [35]. The most important parameters of the superconducting tapes marketed by THEVA, AMSC and SuperPower companies, which must be taken into account in the development of the applications in which these materials are used, are presented in Table 1 [31].

Table 1. Superconducting tape parameters [31].

	Theva Pro-Line TPL2000 [32]	AMSC 8502 [34]	SuperPower SCS12050 [36, 37]	Faraday [35]
Width (mm)	12	12	12	12
I_c (A) at temperature $T = 77$ K	400	300	360	400
Total length (m)	25 – 300	-	200 – 500	10 – 400
Thickness of Cu substrate (μm)	50/100	-	10 – 110	2 x 5
Thickness of Hastelloy (μm)	50	-	30/50	38
Total thickness (μm)	60	180 - 220	100	-
Minimum bend diameter (mm)	30	30	11	10

The SuperPower tape model SCS1250 with 12 mm wide and 0.1 mm thick was selected for the design of the superconducting electromagnet.

2.4. Numerical evaluation of the magnetic field generated by the Helmholtz assembly

Parameters imposed by the application in which the electromagnet must work, presented in Table 2, are determined by the geometric dimensions of the system in which will be mounted.

Table 2. Electromagnet parameters [31].

Inner diameter (D_i)	≤ 70 mm
Outer diameter (D_e)	≤ 200 mm
Magnetic field	5 T
Magnetic field linearity error for $z = \pm 10$ mm (%)	$\leq 0,25$
Working temperature	≤ 77 K

Due to the specific geometry of the superconducting material chosen, to make the electromagnet coils, the pancake configuration will be chosen, each coil of the electromagnet will be made of two double pancake (Figure 4).

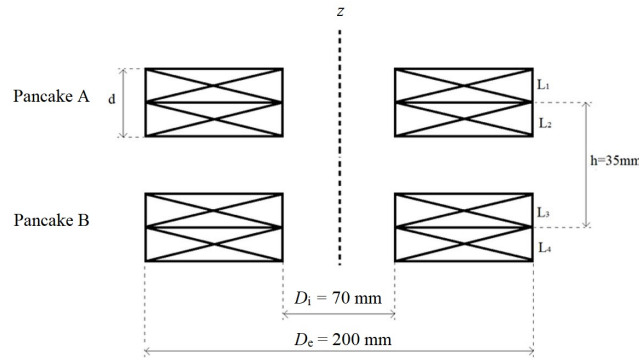


Fig. 4. Helmholtz assembly.

In order to reduce the space between the turns of the coils, non-insulated superconducting tape will be used [31]. Starting from the initial data of the electromagnet presented in Table 2, its geometric parameters were calculated, the resulting values being presented in Table 3.

Table 3. Geometrical parameters of the electromagnet [31].

Fill factor	0,95
Average radius	67,5 mm
Single pancake number of turns	591
Duble pancake number of turns	1182
Total number of turns	2364
Average length of a turn	423,9 mm
Total conductor length	1002,1 m
Heigth of a duble pancake coil d	24 mm

2.4.1. Magnetic field evaluation

For the configuration presented in Figure 5, the parameters $\alpha = 2.857$ and $\beta = 0.342$ were calculated. For distance between the coils $h = D_i/2 = 35$ mm, the magnetic field $B = 5.012$ T was calculated in the center of the assembly ($z = 0, r = 0$) [31], and a supply current $I = 242$ A, the linearity error of 2,1% was obtained for ($r = 0$ and $z = \pm 10$ mm), this value being greater than the value imposed by the application. The distance between the two coils of the

electromagnet was increased to 53 mm, obtaining a magnetic field in the center of the assembly of 5.012 T, corresponding to a supply current of 280 A, the linearity error of the magnetic field for $r = 0$ and $z = \pm 10$ mm being of 0.311%, this value also exceeding the value imposed by the application. Increasing the distance between the coils to 59 mm, a magnetic field of 5.003 T was obtained, the calculated supply current for this distance was 295 A, the linearity error obtained for $r = 0$ and $z = \pm 10$ mm was 0.217 % [31], the results are presented in Figure 5 [31].

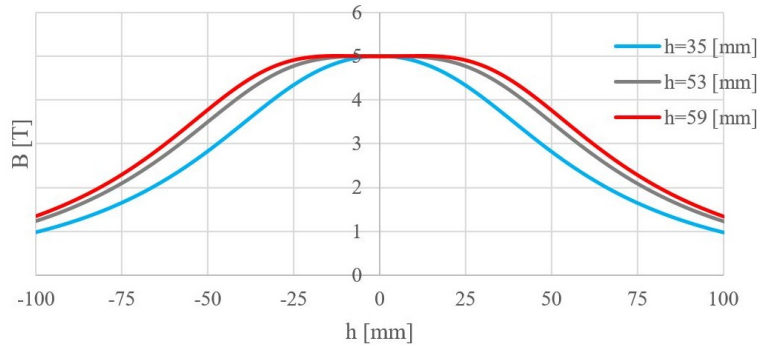


Fig. 5. Magnetic field distribution along Oz axis, calculated for the Helmholtz coil assembly having distance between coils of 35 mm, 53 mm and 59 mm [31].

2.4.2. Magnetic field evaluation trough numerical modeling

Numerical modeling has been carried out for the coil assembly presented in Figure 4. For the coils distance $h = 35$ mm, the magnetic field of 4.978 T was obtained in the center of the assembly ($z = 0$, $r = 0$), and an supply current of 242 A, the magnetic field spectrum obtained trough numerical modeling for the model analyzed is shown in Figure 6. For this model, the relative error between the calculated magnetic field and the one resulting from the numerical modeling is 0.694% [31].

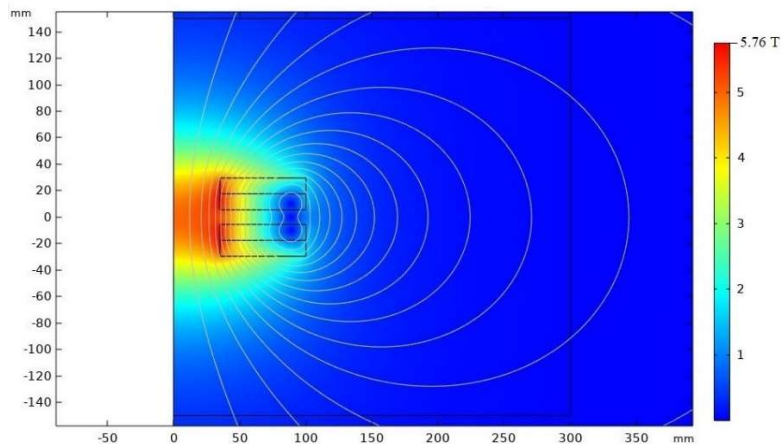


Fig. 6. Magnetic field spectrum obtained trough numerical modeling for the Helmholtz assembly shown in Figure 5 with the coils distance of 35 mm [31].

The numerical modeling was resumed for the distance of 53 mm between the coils of the assembly, a magnetic field of 4.974 T been obtained in its center, and a supply current of 280 A, the relative error between the calculated magnetic field and the value obtained from the numerical modeling being 0.758 % [31].

For distance of 59 mm between the coils of the Helmholtz assembly, a magnetic field of 4.965 T was obtained in the center ($z = 0$, $r = 0$), the supply current in this case being 280 A, the magnetic field distribution obtained trough numerical modeling for this is presented in Figure 7. For this distance, the relative error between the calculated value and the one obtained by numerical modeling is 0.755 % [31].

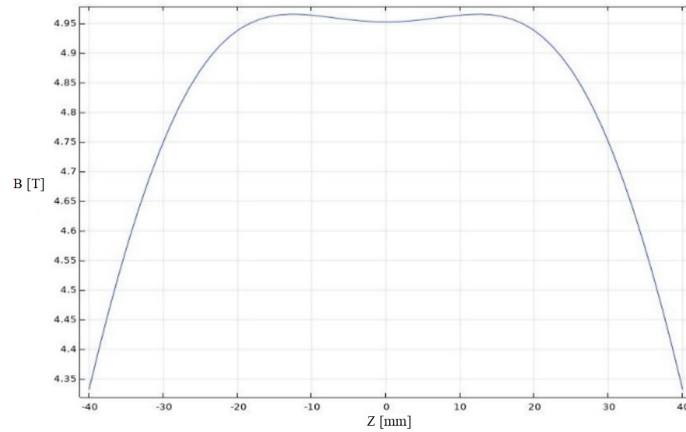


Fig. 7. Magnetic field distribution obtained trough numerical modeling along Oz axis for Helmholtz assembly presented in Figure 5, for the coils distance of 59 mm [31].

2.5. Conclusions

In this chapter, the main elements involved in the design of an electromagnet made with HTS superconducting materials were presented, starting from a conceptual model. When developing this conceptual model, the final characteristics of the electromagnet were taken into account: the maximum magnetic field generated, the geometric dimensions of the area in which the magnetic field is generated, the imposed uniformity of the magnetic field in a certain region. Taking into account that the application for which this electromagnet was designed imposes a region of ± 10 mm along its Oz axis for which the uniformity of the generated magnetic field must be high, the Helmholtz coil assembly was selected for this purpose. In order to make the electromagnet coils, the YBCO type superconducting material was selected. A calculation method for the magnetic field of this coil assembly was also presented, in order to evaluate the optimal distance between the coils for which the linearity error of the field for a given distance is less than 0.25%. The results obtained trough analytical calculation were validated by the numerical modeling, after which a relative error of less than 1% was obtained.

3. THERMAL ANALYSIS PARAMETERS OF THE COOLING SYSTEM FOR THE SUPERCONDUCTING ELECTROMAGNET

3.1. INTRODUCTION

Using LTS or HTS materials in practical applications, implies maintaining their temperature in the range of 4 K – 80 K [38]. The obtaining methods of the cryogenic temperatures depends on the type of superconducting materials used (LTS or HTS) but also the operation time required. The main cooling method used in these type of applications consists in the use of cryogenic agents. Another way to obtain the cryogenic temperatures is through use of heat pumps, generically called cryocoolers [40]. In this chapter, the main methods to obtain the cryogenic temperatures will be presented, as well as sizing the cooling system required for the use of a superconducting electromagnet made with HTS materials.

3.2. Transfer phenomena at low temperatures

The superconducting materials performances, depends directly on the operating thermal regime, the critical parameters of these type of materials having a strong dependence on the temperature. Heat transfer mechanisms are thermal conduction, prevalent in solid and liquid media, convection and thermal radiation.

3.2.1. Thermal conduction

For a thermally conductive material, having surface S_1 connected to a thermostat at temperature T_1 , and surface S_2 connected to a thermostat with temperature T_2 , where $T_1 > T_2$, the rest of the surfaces being thermal isolated, the conduction heat power \dot{Q}_{cond} [W] transferred through a surface S [m²] perpendicular to the temperature gradient is [41]:

$$\dot{Q}_{\text{cond}} = \frac{S}{L} \int_{T_1}^{T_2} k(T) dT. \quad (14)$$

where k [W/mK] is the thermal conductivity of the material, T [K] is the temperature and L [m] the material length. In order to evaluate the conduction heat power \dot{Q}_{cond} , the thermal conduction integrals can be used, they are been available for common materials used in cryogenic applications.

3.2.2. Thermal radiation

An important factor in sizing the cooling system used to obtain the thermal operating regime of equipment used at cryogenic temperatures is heat transfer through radiation. For two parallel surfaces S_1 and S_2 , where $S_1 = S_2$, with emissivities ε_1 and ε_2 and corresponding temperatures T_1 and T_2 respectively, the heat power transferred from surface S_1 to surface S_2 through radiation \dot{Q}_{rad} [W] is [16, 43]:

$$\dot{Q}_{\text{rad}} = \frac{S\sigma(T_1^4 - T_2^4)}{\frac{1}{\varepsilon_1} + \frac{1}{\varepsilon_2} - 1} = \frac{S\sigma(T_1^4 - T_2^4) \varepsilon_1 \varepsilon_2}{\varepsilon_1 + \varepsilon_2 - \varepsilon_1 \varepsilon_2}. \quad (15)$$

3.2.3. Thermal convection

To evaluate the convection heat transfer, a thermal conductive plate is considered, with the surface S at the temperature T_s placed in a fluid whose temperature is T_m , and the velocity (horizontal, uniform) U_{in} . For the case of laminar flow of the fluid, the convective heat flux q_{cv} [Wm^{-2}] is described by Newton's law [42]:

$$q_{cv} = h(T_s - T_m), \quad (16)$$

where h [$Wm^{-2}K^{-1}$] is the convective heat transfer coefficient. Between the surface S of the plate and the *hydrodynamic boundary layer* of thickness δ , the fluid velocity varies between $u = 0$ at the plate surface, up to the velocity $u = 0.99U_{in}$. For viscous fluids, at the wall, the fluid velocity $\mathbf{u} = 0$, the heat exchange between the wall and the fluid (q_s) is carried out through conduction [42].

3.3. Cooling methods

The choice of the cooling method for a system in which superconducting materials are used, in order to keep temperature below the critical temperature (T_c) depends on superconducting material used. For HTS type superconducting materials, the temperature must be maintained in the range of 20 K – 80 K. Another parameter of which directly depends the cooling method to be used is the total heat power required to maintain the system in the desired temperature range. The main cooling methods used in such applications are the use of cryogenic agents and cryocoolers.

3.3.1. Cooling with cryogenic agents

The most common cooling method for superconducting materials is the use of cryogenic agents. An example of this is the cooling achieved by direct immersion of an equipment in a cryostat in which there are liquid cryogenic agents. This method is most often used in laboratory applications where a large cooling power is required. The heat flux between a body surface and the fluid as a function of ΔT_e (the difference between the body surface temperature T_s and the saturated fluid temperature T_{fs}) has a maximum value, known as the critical heat flux ($q_{f,max}$) [43], and minimum, known as leidenfrost point ($q_{f,min}$), and can be evaluated (for cryogenic liquids) using Kutateladze correlation [43].

3.3.2. Heat pumps cooling

A modern method of cooling consists in the use of a heat pump system, called a cryocooler. Different types of cryocoolers are currently commercially available, with heat load varying from a few mW up to 10^{10} W, the main cryocoolers currently used are [44]: JT cryocooler (Joule-Thomson), Bryton cryocooler and Gifford-McMahon cryocooler (GM). The GM cryocooler is a closed circuit heat pump with one or two cooling stages, using helium gas. An example of a cryocooler with two cooling stages is the Sumitomo RDK 415D cryocooler, Figure 8 shows his working diagram For the first stage, heat load corresponding to the temperature of 50 K is 40W respectively 1.5 W for second stage, at temperature of 4.2 K.

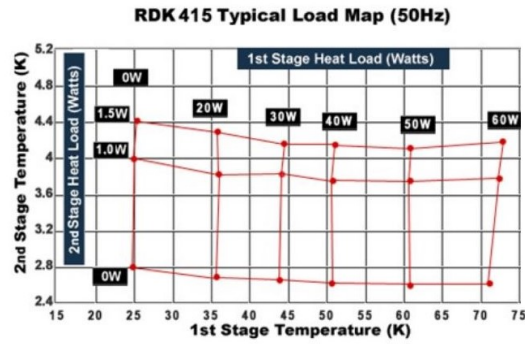


Fig. 8. RDK 415D cryocooler working diagram [45].

3.4. Sizing the cooling system for the HTS superconducting electromagnet

To maintain the HTS superconducting electromagnet at a temperature below the critical temperature of the superconducting material, the radiative heat flux received from the cryostat walls must be evaluated. In order to reduce the radiative heat flux, the electromagnet is covered with a copper thermal shield, which is thermally anchored to the cryocooler. To determine the geometric dimensions of the shield and the cryostat as well as the distances between them, the distance between first stage and second stage of the cryocooler chosen for this application, and the dimensions of the electromagnet will be taken into account. The resulting geometric parameters of the cryostat - shield assembly are presented in Table 5.

Tabele 5. Geometric parameters of the cryostat - shield assembly.

Shield height (mm)	410
Shield outer diameter (mm)	340
Cryostat height (mm)	710
Cryostat outer diameter (mm)	510

3.4.1. Thermal parameters of the cryostat-electromagnet assembly

The HTS superconducting electromagnet, its cooling system and the power supply circuit is shown in Figure 9 [46], the constructive elements of this assembly are: 1. Cryostat; 2. Cryocooler; 3. Current supply connectors; 4. Copper conductors; 5. Thermal shield; 6. HTS conductors; 7. HTS electromagnet.

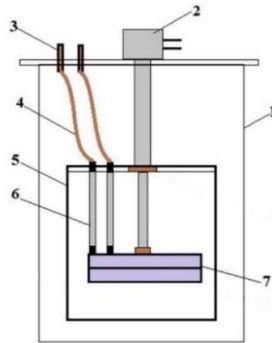


Fig. 9. Circuitul de alimentare pentru un electromagnet supraconductor HTS [46].

3.4.2. Radiative heat flux evaluation

Knowing the surface temperature of the shield ($T_1 = 50$ K) and its emissivity, the surface temperature of the cryostat ($T_2 = 293.15$ K) and its emissivity, the amount of heat absorbed by the shield was calculated, resulting in a power of 8,11 W.

To evaluate the radiative heat flux by numerical modeling, a geometric model was created for the assembly that includes both the cryostat and thermal shield inside it. Following numerical modeling, a radiative power absorbed by the shield of 7.65 W was obtained, the result of this modeling are presented in Figure 10.

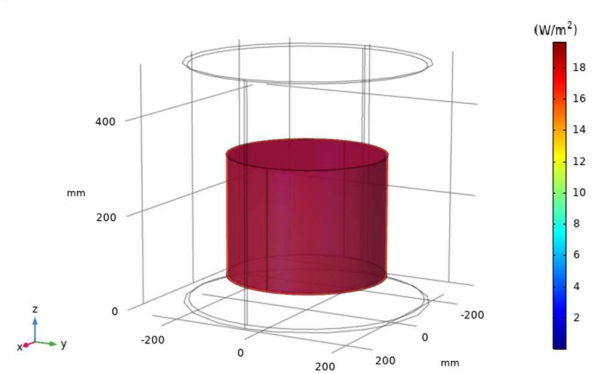


Fig. 10. Shield radiative heat flux [46].

3.4.3. Conductive heat flux evaluation

The copper conductors length is imposed by the distance between the upper part of the thermal shield and the upper flange of the cryostat, which is 190 mm. They are thermally anchored at one end to the shield which is at temperature $T_1 = 50$ K and at the other end to the upper flange of the cryostat at temperature $T_2 = 293.15$ K. The Joule power and conductive heat flux were calculated for different lengths of copper conductors, with the volume being kept constant (Figure 11).

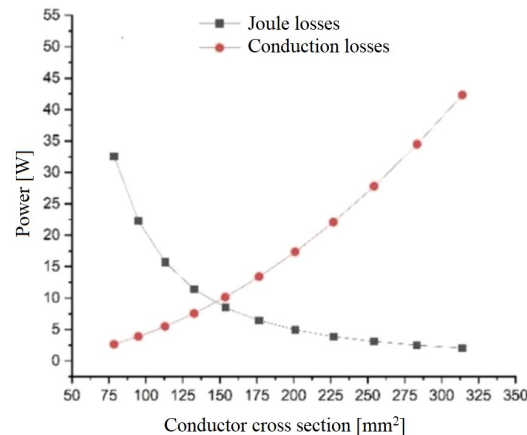


Fig. 11. Joule and conductive power calculated for different conductor cross sections [46].

The optimal cross-section of the copper conductors was determined, for which the total power (Joule and conduction) is 22.368 W, the calculated total thermal power, which also

includes the shield radiative power, is 30.48 W, this value being less than the maximum power available of stage I of the cryocooler, which allows it to operate at a temperature of 50 K. Geometrical models of the supply conductors were made, for different lengths and sections, in order to evaluate Joule and conductive losses. The results obtained for the conductors with a 1619 mm length are presented in Figure 12.

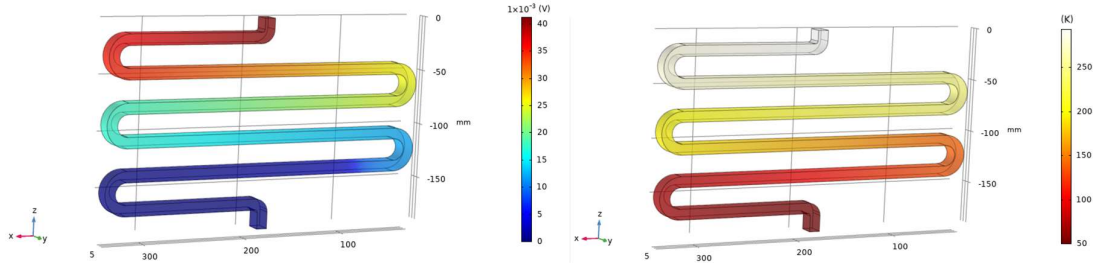


Fig. 12. 1619 mm length conductor, 300 A; electric potential (left) and thermap profile (right) [46].

Figure 13 shows the conductive and Joule losses obtained through numerical modeling for different lengths and cross sections of copper conductors. Following the numerical modeling carried out for different geometries of the conductors, their optimal cross section was determined for which the total heat power (conduction and Joule) is minimal, this being 147.39 mm², with a 1619 mm length, for a power total of 23.019 W. The total heat power of the shield-conductor assembly (which includes radiative power) being 30.669 W.

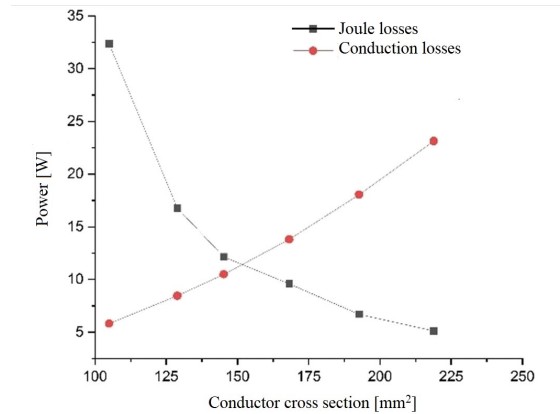


Fig. 13. Joule and conductive heat power obtained through numerical modeling for different conductor cross sections [46].

To evaluate the copper conductors influence on the thermal shield of the electromagnet, numerical modeling was carried out for a geometric model that includes the cryostat-thermal shield assembly together with the two copper conductors. Following this modelling, a total heat power of 35.571 W was obtained for this assembly, which include the radiative, conductive and Joule power. In order to limit the conductive heat flux from the copper conductors to the superconducting electromagnet, the supply circuit between the copper conductors and the electromagnet was made of HTS superconducting tape, this having the lower end thermally anchored to the second stage of the cryocooler and the upper part connected to first stage of the cryocooler. In this configuration, the temperature of the HTS conductor is kept below the critical temperature of the HTS tape (~92 K), ensuring the supply of the electromagnet with

negligible Joule losses, for a supply current of 300 A. In figure 14 [47] the geometric model of the power conductor made with HTS superconducting tape is presented, its constructive elements are: 1. copper terminals; 2. superconducting tape; 3. conductor case.

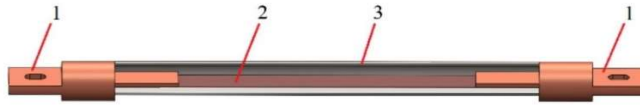


Fig. 14. HTS tape conductor [47].

In order to evaluate the conductive heat flux through this conductor, successive numerical modelings were made for different materials and its thicknesses. Following the numerical modelings, a minimum of 87.01 mW conductive heat power was found for the HTS conductor having the stainless steel case, with 0.5 mm wall thickness [47].

To determine the operating thermal regime of the electromagnet, a geometric model was made for the entire assembly consisting of the thermal shield, the HTS superconducting electromagnet, copper conductors and the HTS conductors. Following numerical modeling, a conductive thermal power of 123.5 mW was found for HTS conductors, and a radiative power of 68.52 mW for the HTS electromagnet. Thus, the total heat power calculated for the HTS electromagnet-conductor assembly is 315.52 mW, which is below the maximum heat load available for the second stage of the cryocooler, which is 1.5 W for 4.2 K.

3.5. Conclusions

In this chapter, the numerical modeling for the power supply system of the HTS superconducting electromagnet was carried out, to determine the optimal copper conductors that are part of the power supply system.

The HTS electromagnet's shield is thermally anchored to first stage of the cryocooler, which receives heat from two sources: radiative, from the cryostat, and conductive, from the two copper conductors. The heat transmitted by copper conductors also has two components: conductive and Joule. Numerical evaluations using the FEM technique revealed the following values for the copper conductors: the length of 1619 mm and a cross section of 147.39 mm². These values were obtained for a total heat power of 35.571 W, the evaluation being carried out taking into account all the thermal effects involved and already listed. The HTS electromagnet and one end of the HTS conductors are thermally connected to the second stage of the cryocooler. Their power (conductive and radiative) obtained through numerical modeling is 367.36 mW, this value being lower than the power available for the second stage of the cryocooler, of 1.5 W for 4.2 K.

Since the powers for the two stages of the cryocooler do not exceed the limit values of 40 W and 1.5 W respectively, the superconducting electromagnet can be cooled with this type of cryocooler.

4. REALIZATION AND TESTING OF THE SUPERCONDUCTING ELECTROMAGNET

4.1. INTRODUCTION

For construction of the HTS superconducting electromagnet, both a mechanical structure to support the coils and a cryostat for the thermal isolation of the electromagnet from the surrounding environment are required. The other constructive elements refer to ensuring the operation thermal regime of the HTS coils, and to their current supply. In this chapter, the method of constructing an HTS electromagnet will be presented, its construction involving a rigorous testing of the superconducting material with which it will be made.

4.2. Mechanical structure of the electromagnet

The realization of the mechanical elements of the electromagnet was made considering its geometrical, electrical and magnetic parameters. The constructive elements of the mechanical structure of the HTS electromagnet (Figure 15) are as follows: 1. central support; 2. electromagnet cover; 3. brackets for spacing pancake pairs; 4. External spacing supports.



Fig. 15. Mechanical support of the HTS electromagnet.

4.3. Superconducting coils execution

For the execution of the pancake coils of the HTS electromagnet, a custom device for this type of winding was designed and made, presented in Figure 16. The high-temperature superconducting material chosen to make the electromagnet winding is a 12 mm and 0.1 mm tape shape, produced by the SuperPower company [36].

To make the pancake coils, the HTS tape (1) wound on aluminum plate (2) is guided by a teflon roller (4). For a uniform distribution of the mechanical tension of the tape, the aluminum plate (2) is connected to a magnetic brake (3) whose torque can be adjusted in the range of 0 – 36 Nm [48]. The electromagnet support the coils (7) is mechanically anchored on the aluminum plate (6), which is driven by an electric motor (5). The HTS tape is distributed symmetrically on two identical plates (2 and 9), the winding of the lower coil being executed using the tape placed on the plate (2), while the second half of the tape needed to make the winding (10) is placed on the plate (9), this being anchored with a metal shaft (8). After making the first coil, the plate (9) containing the tape needed to make the second coil is fixed on the magnetic brake (3), thus continuing the winding of the upper coil. The number of turns for each coil is carried out with an electronic counter equipped with a Hall sensor (11).

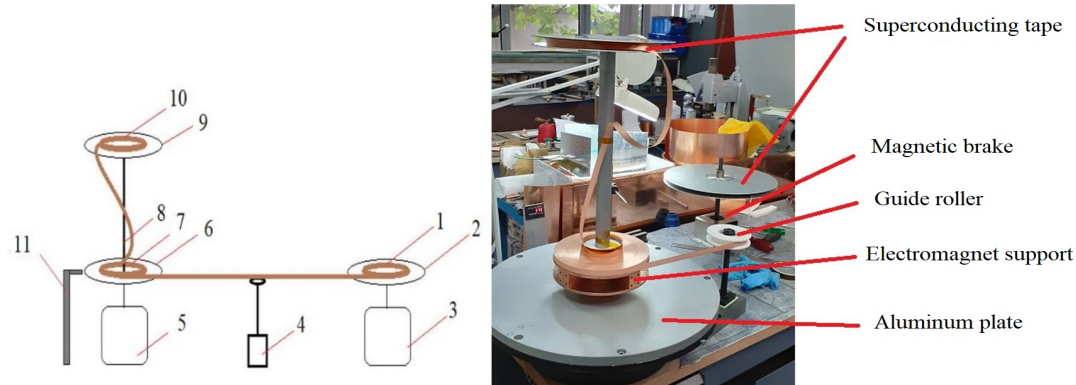


Fig. 16. Diagram of the device used for the HTS electromagnet coils on the left and the image of the device used to make the electromagnet on the right.

4.3.1. Junction of superconducting HTS type

To make a coil in a double pancake configuration, a superconducting tape shape with a length of 501 m is required, the length of the superconducting tape acquired being $\sim 350\text{m}$ [36]. For this, a junction of the THS tape is required. In order to make the tapes junction, a thermostated plate was designed and made, with temperature range is $50\text{ }^{\circ}\text{C} - 300\text{ }^{\circ}\text{C}$ [49]. Figure 17 shows a 12 mm HTS tape junction during tests. The constituent components used for these measurements set-up are as follows: 1. cryostat; 2. support plate; 3. electrical conductors; 4. measuring cable; 5. HTS tape soldered (junctioned). In order to evaluate the superconducting tape junction resistance (Figure 18), successive tests were carried out using different types of solder alloys, for an overlap distance of 100 mm was used. Junction resistance measurement was carried out using a 300 A power supply, and 18.7 μA resolution of the measured current, produced by the American Magnetics was used [50], voltage measurement been performed with Keithley 2182 nanovoltmeter, with 1 nV resolution [51].



Fig. 17. 12 mm HTS tape junctioned, mounted on the testing support plate.

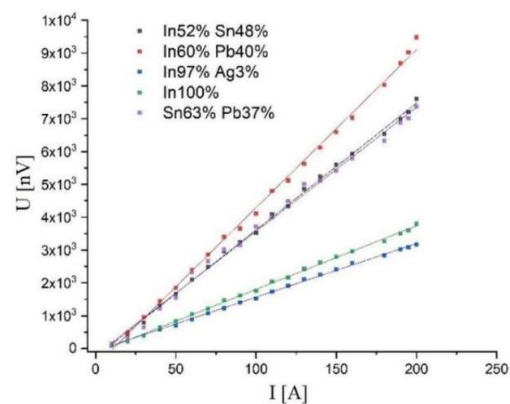


Fig. 18. The resistances values of the 12 mm HTS tape junctions [49].

The AMI 430 a power supply accuracy is 0.015 % for 100 A supply current, and the Keithley nanovoltmeter accuracy is 2.614 %, corresponding to the measured voltage, thus, for the solder alloy 97 % In / 3 %Ag, the resistance calculated was $15.3\text{ n}\Omega \pm 2.63\text{ \%}$.

4.3.2. Current supply conductors

To ensure the supply current of the superconducting electromagnet, copper conductors and HTS type conductors were made. For realization of the HTS conductors, the plate designed to perform the junction of the HTS tapes was used. Figure 19 shows the HTS types conductors without casing, made with the thermostated plate. In order to connect the HTS conductors to the superconducting electromagnet winding (Figure 20), mechanical copper elements (1) were made, these being mechanically anchored on a copper support plate (2), the plate being thermally anchored to the electromagnet support (3), the ends of the electromagnet winding were soldered to these copper elements.



Fig. 19. HTS conductors without casing, made with the thermostated plate.

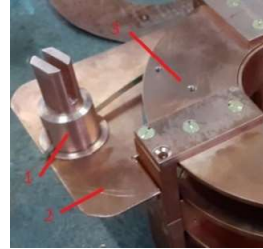


Fig. 20. HTS electromagnet supply current copper elements.

The electrical resistance between the copper terminal of the HTS conductor and the electromagnet terminal was measured after mounting the HTS conductors, and the value of $\sim 300 \mu\Omega$ was obtained.

4.3.3. Electromagnet realization

For the realization of the electromagnet coils, the winding solution with non-insulated superconducting tape was chosen. To insulate the coils from the electromagnet housing, a 0.017 mm thick capton layer was applied between the pair of coils and the upper and lower plates. After completing the winding of the pancake coils, the electrical supply terminals of the electromagnet were mounted (Figure 21.). To measure the temperature of the HTS electromagnet winding, 4 PT100 type platinum temperature sensors were installed, their housing being electrically isolated from the electromagnet housing by means of Teflon gaskets, these sensors being in thermal contact with the superconducting coils (Figure 22).

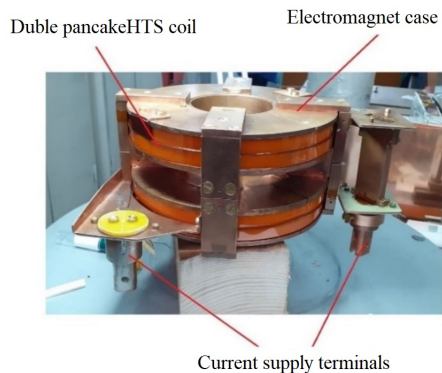


Fig. 21. HTS superconducting electromagnet.

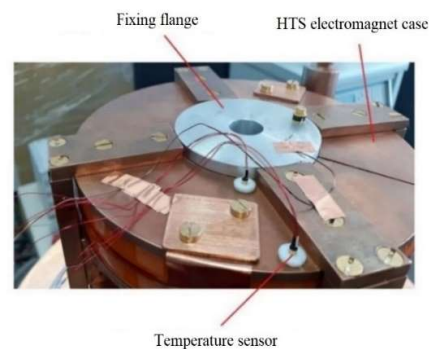


Fig. 22. Temperature sensors mounted on the HTS electromagnet.

4.4. Cryogenic cooling system

The electromagnet's cryogenic cooling system is based on the use of a Gifford-McMahon RDK415D cryocooler. It has two cooling stages, with temperatures of 50 K and 4.2 K respectively, the electromagnet being conduction cooled. The cryogenic cooling system of the electromagnet consists of a vacuumed cryostat, the pressure value being $\sim 10^{-6}$ mbar, in which the cold head of the cryocooler is mounted, ensuring the cooling of the superconducting electromagnet and also the thermal shield.

4.4.1. Cryostat

To to ensure the temperature operating regime of the superconducting electromagnet in order to test it, a cryostat was made from non magnetic stainless steel OL304, with an inner diameter of 500 mm and a height of 710 mm, and a wall thickness of 5 mm (Figure 23). In the upper part, the cryostat is provided with a 10 mm diameter flange for access of the Hall probe needed to measure the electromagnet magnetic field.

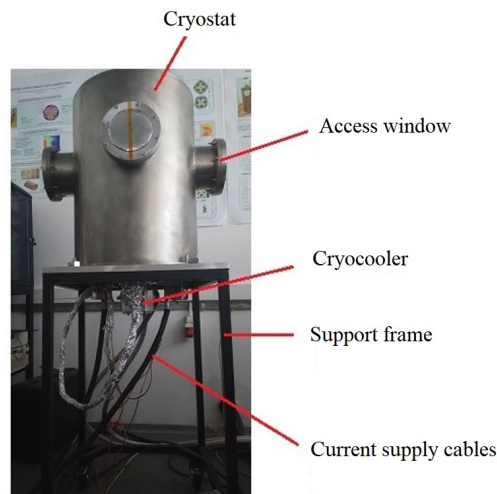


Fig. 23. The cryostat mounted on the support frame.

4.4.2. Thermal shield

The thermal shield made of copper, with 1 mm thickness protects the HTS superconducting electromagnet from the radiative heat flux emitted by the cryostat walls. Its lower part is thermally anchored to the first stage of the cryocooler, which is at 50 K. In the upper part, it is provided with a 10 mm diameter hole, for Hall probe access, needed to measure the magnetic field generated by the superconducting electromagnet. Due to the fact that copper oxidizes over time, considerably increasing its emissivity, the shield was covered at the outside with aluminized mylar, to ensure a low emissivity.

4.5. Experimental tests

In order to establish the HTS superconducting electromagnet performance, an experimental test system was created (Figure 24) to ensure its optimal operating conditions, the constructive elements are: 1- Cryostat flange; 2- Vacuumed enclosure (cryostat); 3- Thermal shield; 4- G-M Cryocooler; 5- Electromagnet support plate; 6- Copper esupply

conductors; 7- HTS electromagnet; 8- HTS conductors; 9- Cryogenic Hall probe; 10- Support frame.

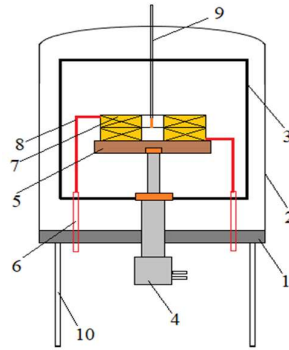


Fig. 24. HTS electromagnet experimental test system [52].

4.5.1. Testing the HTS tapes

The HTS tape used for HTS electromagnet was delivered in lengths of ~ 350 m. Each of the tape sectors is wound on aluminum support to ensure adequate mechanical protection. For each batch purchased, preliminary tests were carried out in order to determine the critical currents. Figure 25 shows an aluminum support with 350 m of superconducting tape under test. The HTS tape mounted on aluminum support (1) is placed on a copper plate (2) which is thermally anchored to the cryocooler second stage, the supply current being assured by the copper conductors (3), the electrical conductors used to measure the voltage (4) are soldered directly on the superconducting tape, the tapes being tested for a maximum current of 350 A. After critical current measurements, the average value of $0.51 \text{ n}\Omega \pm 43.8\%$ was obtained, the critical current I_c corresponding to the electric field threshold of $1 \text{ }\mu\text{V}/\text{cm}$ not being obtained [36] (Figure 26).



Fig. 25. 12 mm HTS tape tested.

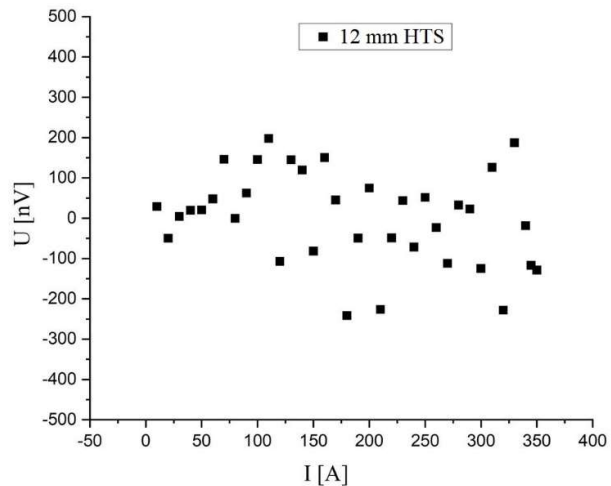


Fig. 26. Measured voltage as a function of supply current for 12 mm width and 350 m long HTS tape.

4.5.2. HTS electromagnet testing system

The measurement chain used to test the superconducting electromagnet (Figure 27) consist of the following elements: 1. Power supply, model AMI 430 with a maximum supply current of 500 A [50]; 2. LakeShore temperature monitor model 218 [53]; 3. Keithley 2182 nanovoltmeter [51]; 4. LakeShore DSP475 gaussmeter [53]; 5. PC unit.



Fig. 27. The measurement chain used to test the HTS electromagnet.

4.5.3. Experimental results

The superconducting electromagnet was subjected to cryogenic tests, the temperatures of the coils and the temperature of the second stage of the cryocooler were measured, the temperature sensors location being presented in Figure 28. 5 temperature sensors were used, the first sensor, mounted at the second stage of the cryocooler is a LakeShore DT670 silicon diode [53], with a minimum temperature of 1.4 K, and an accuracy of ± 12 mK. The sensors used to measure the temperature of the electromagnet winding are platinum thermoresistances, with a temperature range of 14 K – 873 K, and ± 20 mK accuracy. The electromagnet cooling was evaluated for 3 days, the temperature of the winding of the electromagnet was in the range of 24 K and 42 K, the temperature of the cryocooler second stage reached the value of 16 K. After cooling, the electromagnet was powered up with the supplied current of 295 A. Figure 29 shows the temperature variation of the electromagnet during operation.

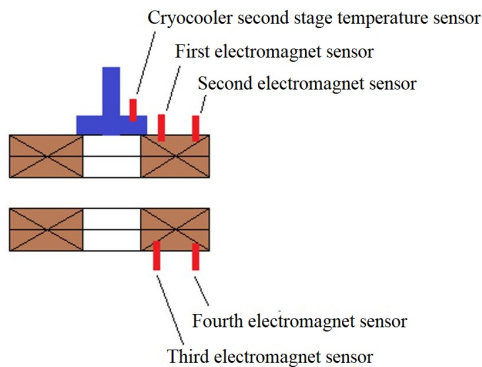


Fig. 28. The location of the temperature sensors of the HTS electromagnet.

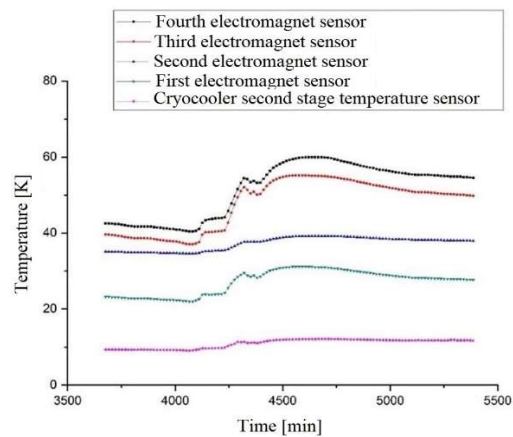


Fig. 29. Temperature of the HTS electromagnet coils.

The temperature of its lower coil, being the furth from the cryocooler second stage, presents a larger temperature variation compared to the temperature of the upper coil. The increase in the temperature of the electromagnet, followed by a gradual cooling, is due to the heat produced by the Eddy currents induced in the electromagnet copper casing, due to the variation of the supply current.

To determine the magnetic field generated by the HTS superconducting electromagnet as a function of supply current, an axial cryogenic Hall probe, produced by the LakeShore company, model HMCA-2560-WN, with measuring range of 3.5 mT – 35 T and $\pm 2\%$ of the measured value accuracy was used. This probewas connected to a LakeShore Gaussmeter model DSP475, the measurement accuracy being $\pm 0.05\%$ of the reading value and 0.005% of the measurement range, and the resolution of 0.1 mT for 35 T range. Thus, for a supply current of 295 A, the magnetic field measured was 5,05 T.

After reaching the supply current value to the HTS electromagnet of 295 A, the Hall probe was moved in the direction of the Oz axis, for $\Delta z = \pm 28$ mm, in order to evaluate the uniformity of the magnetic field generated along this axis. Figure 30 shows the graph with the results of magnetic field measurements on the Oz axis, centered at the origin ($z = 0, r = 0$). An asymmetry of the magnetic field of 7.1 mT was found, this being due to errors in the execution process of the coils, corresponding to the two double pancakes.

In order to evaluate the uniformity of the magnetic field measured in the center of the HTS electromagnet (Figure 31) along the Oz axis, for the distance of ± 10 mm from its center ($z = 0, r = 0$) the linearity error was calculated, the value of 0.112 % being obtained at the distance of +10 mm, and for the distance of -10 mm 0.059 % was obtained, the value imposed by the application for the distance of ± 10 mm being $\leq 0.25\%$.

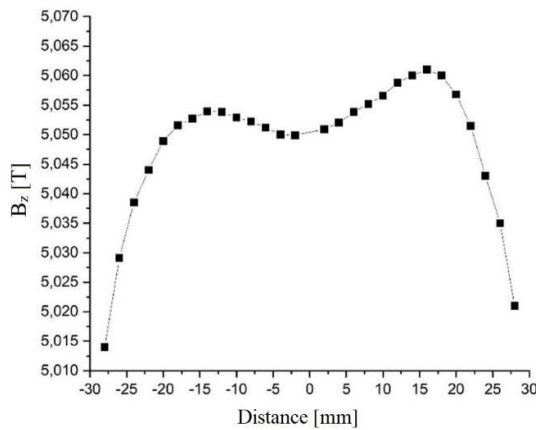


Fig.30. Magnetic field distribution measured along Oz axis for the HTS superconducting electromagnet.

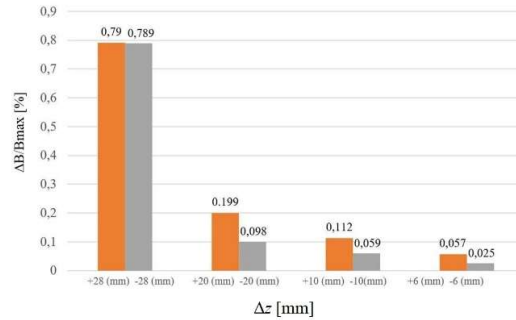


Fig. 31. Linearity error calculated for the mgnetic field generated along the Oz axis.

In chapter 2, the magnetic field of 5.003 T generated by the HTS coil assembly was calculated for a supply current value of 295 A, the linearity error calculated for $\Delta z = \pm 10$ mm from the origin ($r = 0, z = 0$) being 0.217%. Figure 32 shows the values of the calculated magnetic field and the measured magnetic field, for $r = 0$, and $\Delta z = \pm 28$ mm. The relative error between the two values of the magnetic field (calculated and measured) is 1.13 %.

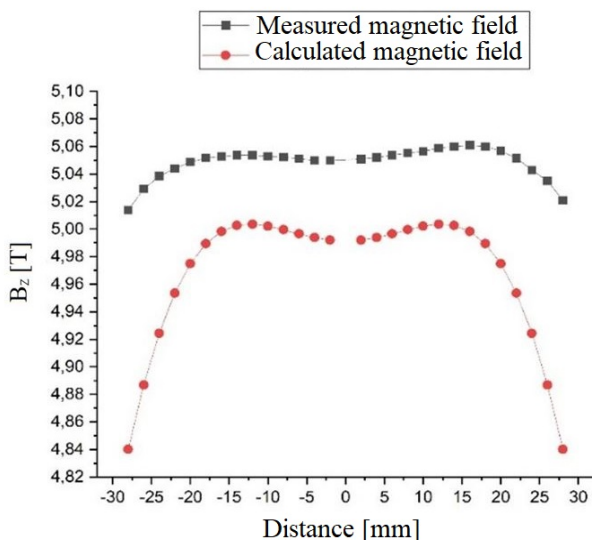


Fig. 32. Magnetic field distribution (measured and calculated) along Oz axis.

4.6. Conclusions

In this chapter, the realization and testing stages of an electromagnet in Helmholtz configuration made with high-temperature superconducting materials were presented. In order to obtain the necessary length needed for the realization of the electromagnet coils, tape junctions was performed, the experimentally obtained value of the superconducting tape junction resistance is $\sim 15 \text{ n}\Omega$ for the In 97 % Ag 3 % alloy. The cryogenic tests was performed for the HTS electromagnet, the measured temperature of the superconducting coils was between 24 K and 42 K, the cryocooler second stage temperature being 16 K. As the critical temperature T_c of the superconducting tape (92 K) was not exceeded, the electromagnet can be maintained in the superconducting state indefinitely. During the tests of the HTS superconducting electromagnet, the magnetic field generated by it was measured for different values of the supply current. Thus, for a supply current of 295 A, the magnetic field along the Oz axis, for $r = 0$, a minimum of 5.05 T and a maximum of 5.06 T was measured. The magnetic field linearity error along the Oz axis is 0.112% for distance of +10 mm, respectively 0.059% for -10 mm, the values obtained being lower than the value imposed by the application for ± 10 mm distance, which is $\leq 0.25\%$. Following the magnetic field measurements made for this electromagnet, for the distance $\Delta z = \pm 15$ mm from center ($z = 0$, $r = 0$), an asymmetry of 7.1 mT was found, this being caused by the errors that occurred in the execution process of the coils corresponding to the two double pancake coils, the relative error between the experimentally obtained magnetic field and the calculated values is 1.13%.

5. CONCLUSIONS

C.1. General conclusions

In Chapter I, the phenomena that govern the superconducting state of materials and the parameters of these types of materials are presented, such as the critical field B_c , critical current I_c and critical temperature T_c , which practically determine the classification of these materials. Depending on the temperature, three categories of superconducting materials are distinguished: low temperature superconducting materials (LTS), which impose the use of liquid helium, medium temperature superconducting materials (MTS) and high temperature superconducting materials (HTS). Also, the main applications were presented in which these type of materials were imposed by their superior performance compared to conventional materials.

In Chapter II the main elements involved in the design of an electromagnet made with high temperature superconducting materials were presented. Also, the main characteristics of HTS superconducting materials available on the market were presented. Following their analysis, the type of material used for designing and execution of the HTS electromagnet was selected.

Also, a calculation method was presented for the evaluation of the magnetic field produced by the superconducting electromagnet, taking into account its geometric parameters, the configuration of double pancake being chosen to make the coils of the electromagnet, due to the geometrical restrictions of the superconducting tape on the one hand, but and the geometric constraints imposed by the application in which this electromagnet will operate.

For this electromagnet, a geometric model was created in order to numerically evaluate by the finite element method the magnetic field depending on the supply current, with a relative error less than 1% between the results obtained by numerical modeling and calculated values.

In Chapter 3, the main cooling methods used for such applications were evaluated, and a Gifford-McMahon type closed circuit cryocooler, with two cooling stages, first stage having a heat load of 40 W corresponding to the temperature of 50 K, and the second stage having 1.5 W for the temperature of 4.2 K was chosen as the cooling solution to ensure the thermal operating regime of the electromagnet.

Due to the low heat load available for the two stages of the cryocooler, the heat powers (conduction and Joule) for the electromagnet supply conductors were evaluated, both the length and the optimal section for which the losses are minimal being determined, the total heat power of the two conductors being 23.019 W.

Due to the low temperature of the electromagnet (4.2 K), it needs to be covered with a copper shield, which is connected to first stage of the cryocooler. The radiative heat flux was evaluated for this shield, the value obtained being 7.65 W. HTS type supply conductors capable of withstanding high supply currents (~ 300 A) have been designed, the conductive heat power of such a conductor being evaluated at 87, 01 mW.

A 3D model of the entire assembly consisting of a cryostat, electromagnet shield, superconducting electromagnet, copper conductors and HTS conductors was made, in order to evaluate the total heat load, a heat load (radiative and conductive) of 315.52 mW for the HTS electromagnet was obtained, and a total heat load (conductive, radiative and Joule) of 35.571 W for electromagnet shield and copper conductors was found.

In chapter 4, the actual realization of the superconducting electromagnet is presented. An experimental study was carried out on the possibility of joining superconducting tape sectors,

the resistance obtained using the soldering alloy In 97 % Ag 3% for these junctions being $\sim 15.3 \text{ n}\Omega$, corresponding to a power of $\sim 2.61 \text{ mW}$ for a supply current of 295 A. Cryogenic tests were also carried out for the HTS electromagnet, the temperature measured of its coils being in the range of 24 K and 42 K. Taking into account that the critical temperature of the superconducting tape used is $\sim 92 \text{ K}$, the HTS electromagnet can work for long periods of time.

Following the magnetic field measurements for this electromagnet, a value of the magnetic field of 5.05 T in the center was obtained, corresponding to an current of 295 A. Following the magnetic field measurements made along the Oz axis ($\Delta z = \pm 10 \text{ mm}$), the linearity error obtained was 0.112 %, this value being lower than the value imposed by the application for which this electromagnet was designed ($\leq 0.25 \%$). For the $\Delta z = \pm 15 \text{ mm}$, an asymmetry of the magnetic field of 7.1 mT was found, a possible cause of this asymmetry being errors in the process of mechanical execution of the constructive elements of the electromagnet.

C.2. Original contributions

The PhD thesis entitled "*Cryoelectrotechnical methods for high magnetic fields*" presents the design and realization of an intense and uniform magnetic field generator made with high temperature superconducting materials.

The original contributions of the thesis are:

- a synthesis of the superconducting materials parameters, needed in order to select the types of usable materials according to the nature of the application in which they are to be used;
- designing and execution of a Helmholtz configuration HTS superconducting electromagnet that can work for time periods that can reach tens of thousands of hours, without the need for refueling with cryogenic agents or any type of maintenance;
- the experimental study of superconducting junctions of the HTS tapes, in order to determine the soldering alloy and the optimal conditions of realization, for which their electrical resistance is minimal, in order to limit the Joule power dissipated by them;
- the design and execution of mixed power supply conductors (Copper – HTS) for the superconducting electromagnet, to minimize conductive heat flux and Joule losses.
- creating a model for calculating the magnetic field generated by the superconducting electromagnet, which I validated through numerical modeling;
- a numerical model of the entire cryostat-electromagnet assembly;
- a numerical model for the design and testing of the HTS conductors required to reduce the conductive heat flux to the superconducting electromagnet;
- the design, realization and testing of a cryogenic cooling system used to ensure the thermal regime and operation of the superconducting electromagnet.

C.3. Development perspectives

New HTS materials with high electrical and magnetic performance are increasingly used to develop superconducting electromagnets generating high magnetic fields, used in experimental physics applications (particle accelerators) or in medicine (medical imaging) or high-speed transport (MAGLEV trains).

In perspective, related phenomena that may appear in the operation of superconducting windings will be addressed and studied experimentally: the influence of the magnetization of the material and the screening currents, on the generated magnetic.

6. BIBLIODRAPHY

- [1] Seok Ju Lee, Minwon Park, In-Keun Yu, Youngjin Won, Yangho Kwak și Chulhyu Lee, „Recent Status and Progress on HTS Cables for AC and DC Power Transmission in Korea,” *APPLIED SUPERCONDUCTIVITY*, vol. 28, nr. doi: 10.1109/TASC.2018.2820721, 2018.
- [2] S.W. Schwenterly, B.W. McConnell, J.A. Demko, A. Fadnek, J. Hsu, F.A. List, M.S. Walker, D.W. Hazelton, F.S. Murray, J.A. Rice, C.M. Trautwein, X. Shi, R.A. Farrell, J. Bascuiian, R.E. Hintz, S.P. Mehta, N. Aversa, J.A. Ebert, B.A. Bednar, D.J. Neder, A.A. McIlheran, P.C. Michel, J.J. Nemeč, E.F. Pleva, R.C. Longsworth, R.C. Johnson, R.H. Jones, J.K. Nelson, R.C. Degeneff și S.J. Salon , „Performance of a 1-MVA HTS Demonstration Transformer,” *IEEE TRANSACTIONS ON APPLIED SUPERCONDUCTIVITY, VOL. 9, NO. 2, JUNE 1999*, nr. doi: 1051-8223/99\$10.00.
- [3] Jianxun Jin și Xiaoyuan Chen, „Development of HTS Transformers,” *2008 IEEE International Conference on Industrial Technology, Chengdu, 2008, pp. 1-6, , nr. doi: 10.1109/ICIT.2008.4608455..*
- [4] Joachim Bock, Achim Hobl, Simon Krämer și Mark O Rikel, „HTS Fault Current Limiters—First Commercial Devices for Distribution Level,” *IEEE Transactions on Applied Superconductivity · July 2011*, nr. DOI: 10.1109/TASC.2010.2099636.
- [5] S.S. Kalsi, D. Aized, B. Connor, G. Snitchler, J. Campbell, R.E. Schwall, J. Kellers, Th. Stephanblome și A. Tromm, „HTS SMES Magnet Design and Test Results,” *IEEE TRANSACTIONS ON APPLIED SUPERCONDUCTIVITY, VOL. 7, NO. 2, JUNE 1997*, nr. doi: 10.1109/77.614667.
- [6] Shinji Matsumoto, Tsukasa Kiyoshi, Gen Nishijima, Kenjiro Hashi, Masato Takahashi, Takashi Noguchi, Shinobu Ohki, Hideaki Maeda și Tadashi Shimizu, „Equipment for Power Outage in Operation of Driven-Mode NMR Magnet,” *IEEE TRANSACTIONS ON APPLIED SUPERCONDUCTIVITY, VOL. 26, NO. 4, JUNE 2016*, nr. vol. 26, no. 4, pp. 1-4, June 2016, Art no. 4301004, doi: 10.1109/TASC.2016.2519515..
- [7] M. I. Faley, U. Poppe, R. E. Dunin-Borkowski, M. Schiek, F. Boers, H. Chocholacs, J. Dammers, E. Eich, N. J. Shah, A. B. Ermakov, V. Y. Slobodchikov, Y. V. Maslennikov și V. P. Koshelets, „superconducting magnetoencephalography,” *IEEE TRANSACTIONS ON APPLIED SUPERCONDUCTIVITY, VOL. 23, NO. 3, JUNE 2013*, nr. doi: 10.1109/TASC.2012.2229094.
- [8] Kazuo Sawada, „Outlook of the Superconducting Maglev,” *in Proceedings of the IEEE, vol. 97, no. 11, pp. 1881-1885, Nov. 2009, , nr. doi: 10.1109/JPROC.2009.2030246..*
- [9] CERN, „CERN Accelerating science,” [Interactiv]. Available: <https://home.cern/science/engineering/restarting-lhc-why-13-tev>. [Accesat 04 2024].
- [10] H. Seungyong, K. Kwanglok, K. Kwangmin, H. Xinbo, P. Thomas, D. Iain, K. Seokho, R. B. Kabindra, N. So, J. Jan și C. L. David , „45.5-tesla direct-current magnetic field generated with a high-temperature superconducting magnet,” *LETTER*, nr. <https://doi.org/10.1038/s41586-019-1293-1>.
- [11] P. Schmuser, Superconductivity, Institut fur Experimentalphysik der Universitat Hamburg: <https://www.desy.de/~pschmues/Superconductivity.pdf>.
- [12] P. H. Rudolf , „The Path to Type-II Superconductivity,” *MDPI metals*, nr. 682, p. 9, 2019.
- [13] A. M. Forrest, "Meissner and Ochsenfeld revisited," *European Journal of Physics, Volume 4, Number 2*, vol. 4, no. 2, pp. 1-5, 1983.
- [14] D. Guillaume, Etude expérimentale et numérique des courants d'e' crantage dans les aimants supraconducteurs a' haute tempe' rature critique REBCO, Grenoble, France: Université Grenoble Alpes (ComUE), 11.10.2017.
- [15] C. Poole, H. Farach și R. Creswick, Handbook of Superconductivity, eBook ISBN: 9780080533216: Academic Press, 15th October 2000.

- [16] Y. Iwasa, *Case Studies in Superconducting Magnets: Design and Operational Issues*, Springer Science + Business Media, LLC 2009: DOI: 10.1007/b112047_1.
- [17] Voicu Dolocan, „SUPRACONDUCTIBILITATEA PRINCIPIILE FIZICE ȘI APLICAȚII,” *EDITURA UNIVERSITĂȚII DIN BUCUREȘTI*, nr. ISBN-973-575-069, 1997.
- [18] A.G. Shepelev, „The Discovery of Type II Superconductors (Shubnikov Phase),” *Superconductor*, 2010, doi: 10.5772/10117.
- [19] Teruo Matsushita, *Flux Pinning in Superconductors*, Library of Congress Control Number: 2006933137, Springer-Verlag Berlin Heidelberg 2007.
- [20] T. Boutboul, S. Le Naour, D. Leroy, L. Oberli and V. Previtali, "Critical Current Density in Superconducting Nb-Ti Strands in the 100 mT to 11 T Applied Field Range," *19th International Conference on Magnet Technology (MT19)*, 18-23.09.2005, Genova, Italy, <https://cds.cern.ch/record/970378/files/lhc-project-report-885.pdf>.
- [21] The Slovenian Academy of Sciences and Arts (SASA), „SLOVENSKA AKADEMIJA ZNANOSTI IN UMETNOSTI,” [Interactiv]. Available: <https://www.sazu.si/en/members/karl-alexander-muller>.
- [22] L. Cooley and I. Pong, "Cost drivers for very high energy p-p collider magnet conductors," Fermilab, FCC 2016, <https://slideplayer.com/slide/11550286/>, Rome, Italy.
- [23] P. M. Grant și T. P. S. Epri, „Cost Projections for High Temperature Superconductors,” Applied Superconductivity Conference, Palo Alto and Palm Desert, California, September 1998.
- [24] "Superconducting Power Cable," *Cryogenic & Vacuum Engineering (CVE)*, [Online]. Available: <https://www.cve.co.kr/en/project/m1513/>. [Accessed 2021].
- [25] W. Goldacker, F. Grilli, E. Pardo, A. Kario, Schlachter, S. I. Schlachter și M. Vojenčiak, „Roebel cables from REBCO coated conductors: a one-century-old concept for the superconductivity of the future,” *Superconductor Science and Technology*, vol. 27, nr. 9, 2014.
- [26] Dr Nick Long, „Roebel cable industrial optimization - General Cable Superconductors,” 2014. [Interactiv]. Available: https://indico.cern.ch/event/308828/contributions/1680710/attachments/589811/811815/WA_MHTS-1_presentation_GCS_May_2014-N.Long.pdf.
- [27] J. KLARKE, „Low-Frequency Applications OF Superconducting Quantum Interference Devices,” Vol. %1 din %2PROCEEDINGS OF THE IEEE, VOL. 61, NO. 1, 1973.
- [28] D. E. G. D. A. D. Dobrin Ion, *Aplicatii ale supraconductibilitatii in ingineria electrica*, ed. Electra, Bucuresti, 2020, ISBN 978-606-507-129-2.
- [29] M. P. Edward, "BERKLEY PHYSICS COURSE," in *Magnetism and Electricity*, 1982.
- [30] D. Bruce Montgomery, *Solenoid Magnet Design*, New: Robert Krieger Publishing, 1980.
- [31] George DUMITRU, Ion DOBRIN și Dan ENACHE, „PROIECTAREA UNUI ELECTROMAGNET SUPRACONDUCTOR HTS GENERATOR DE CÂMP MAGNETIC INTENS ȘI UNIFORM,” *APME*, Vol. %1 din %218, 1, pp. 125-135, 2022, nr. ISSN / ISSN-L: 1843-5912.
- [32] „Theva,” [Interactiv]. Available: https://www.theva.de/wp-content/uploads/2021/05/210412_Flyer_Supraleiter_A5_THEVA_small.pdf. [Accesat 2021].
- [33] „FURUKAWA ELECTRIC GROUP,” [Interactiv]. Available: <https://www.furukawa.co.uk/products/super-conductor/>. [Accesat 2024].
- [34] „Amesc,” Available: <https://www.amsc.com/gridtec/amperium-hts-wire/>. [Accesat 2021].
- [35] „FARADAY FACTORY,” Available: <https://www.faradaygroup.com/en/>. [Accesat 2024].
- [36] SuperPower, „Superpower Inc.,” [Interactiv]. Available: <https://www.superpower-inc.com/specification.aspx>. [Accesat 2021].

- [37] A. W. Zimmermann și S. M. Sharkh, „Design of a 1 MJ/100 kW high temperature superconducting magnet for energy storage,” *Faculty of Engineering and Physical Sciences, University of Southampton, Highfield Campus, Southampton, SO17 1BJ, UK*, 22 March 2020.
- [38] R. Raderburgh, Refrigeration of superconductors, National Institute of Standards and Technology, CO 80305 USA, PROCEEDINGS OF THE IEEE, VOL. 92, NO. 10, 2004.
- [39] A. Ishiyama, M. Yanai, T. Morisaki, H. Ueda, S. Akita, S. Kouso, Y. Tatsuta, H. Abe și K. Tasaki, „Transient Thermal Characteristics of Cryocooler-Cooled HTS Coil for SMES,” *IEEE TRANSACTIONS ON APPLIED SUPERCONDUCTIVITY, VOL. 15, NO. 2, JUNE 2005*, nr. doi: 10.1109/TASC.2005.849321.
- [40] K. Watazawa, J. Sakuraba, F. Hata, T. Hasebe, C.K. Chong și Y. Yamada, „A Cryocooler Cooled 6T NbTi Superconducting Magnet with Room Temperature Bore of 220 mm,” *IEEE TRANSACTIONS ON MAGNETICS, VOL. 32, NO. 4, JUL. 1996*, nr. doi: 10.1109/20.511404.
- [41] W. E. Jack, EXPERIMENTAL TECHNIQUE FOR LOW TEMPERATURE MEASUREMENTS, National Institute of Standards and Technology, Boulder, CO, USA: Oxford University Press 2006, ISBN 0-19-857054-6 978-0-19-857054-7, 2006.
- [42] A. M. Morega, Principles of Heat Transfer, chapter VII in Mechanical Engineer’s Handbook, Bucharest: Ed. Marghitu D.B., Academic Press, 2001, p. 446-557.
- [43] FRANK P. INCROPERA, DAVID P. DEWITT, THEODORE L. BERGMAN și ADRIENNE S. LAVINE, Fundamentals of Heat and Mass Transfer, 6th ed. ISBN 13 978-0-471-45728-2.
- [44] RAY RADEBAUGH, Refrigeration for Superconductors, Cryogenic Technologies Group, National Institute of Standards and Technology, Boulder, CO 80305 USA: PROCEEDINGS OF THE IEEE, VOL. 92, NO. 10, OCTOBER 2004, April 21, 2004.
- [45] Michael A. Green, Magnet and Absorber Heat Loads Cooling with Various Small Coolers, University of Oxford Department of Physics Oxford OX1 3RH, UK, 18.06.2004.
- [46] George Dumitru, Alexandru Morega, Ion Dobrin, Dan Enache și Adrian Nedelcu, Analysis of the thermal and electrical parameters of the supply system of an HTS superconducting electromagnet, Iasi: 2022 International Conference and Exposition on Electrical And Power Engineering (EPE) | 978-1-6654-8994-2/22/\$31.00 ©2022 IEEE | DOI: 10.1109/EPE56121.2022.9959852 , 2022.
- [47] George Dumitru, Alexandru-Mihail Morega, Ion Dobrin, Dan Enache și Constantin Dumitru, „THE DESIGN OF THE POWER SUPPLY CURRENT LEADS TO A HIGH-TEMPERATURE SUPERCONDUCTING ELECTROMAGNET,” *Rev. Roum. Sci. Techn.–Électrotechn. et Énerg.* Vol. 68, 4, pp. 431–435, Bucarest, 2023, DOI: 10.59277/RRST-EE.2023.68.4.18.
- [48] M. T. LTD, „<https://www.magnetictech.com/products/>,” [Interactiv].
- [49] GEORGE DUMITRU, ALEXANDRU-MIHAIL MOREGA, ION DOBRIN, DAN ENACHE și CONSTANTIN DUMITRU, „THE DESIGN OF THE POWER SUPPLY CURRENT LEADS TO A HIGH-TEMPERATURE SUPERCONDUCTING ELECTROMAGNET,” *Rev. Roum. Sci. Techn.–Électrotechn. et Énerg.*, vol. 68, nr. Vol. 68, 4, pp. 431–435, Bucarest, 2023, DOI: 10.59277/RRST-EE.2023.68.4.18.
- [50] <http://www.americanmagnetics.com/power.php>.
- [51] <https://www.tek.com/en/products/keithley/low-level-sensitive-and-specialty-instruments/nanovoltmeter-model-2182a>.
- [52] Dan ENACHE, George DUMITRU, Ion DOBRIN și Mihai GUȚU, „A Measuring System for HTS Wires and Coils Properties at Low Temperatures,” *Electrotehnica, Electronica, Automatica (EEA)*, Vol. %1 din %2 vol. 71 (2023), nr. 3, pp. 03-11, nr. <https://doi.org/10.46904/eea.23.71.3.1108001>.
- [53] L. S. Cryotronics, „<https://www.lakeshore.com/products/categories/specification/temperature-products/cryogenic-temperature-sensors/dt-670-silicon-diodes/>,” [Interactiv].